# Investigation of Ultrasound-Measured Flow Velocity, Flow Rate and Wall Shear Rate in Radial and Ulnar Arteries Using Simulation

# ORIGINAL CONTRIBUTION: INVESTIGATION OF ULTRASOUND-MEASURED FLOW VELOCITY, FLOW RATE AND WALL SHEAR RATE IN RADIAL AND ULNAR ARTERIES USING SIMULATION

XIAOWEI ZHOU* CHUNMING XIA‡, GANDY STEPHEN‡, FAISEL KHAN§, GEORGE A CORNER*, PETER R HOSKINS†, and ZHIHONG HUANG*

*School of Science and Engineering, University of Dundee, Dundee, United Kingdom

† Centre for Cardiovascular Science, University of Edinburgh, Edinburgh, United Kingdom

§ Cardiovascular and Diabetes Medicine, Ninewells Hospital and Medical School, University of Dundee, Dundee, United Kingdom

‡ School of Mechanical and Power Engineering, East China University of Science and Technology, Shanghai, China

‡ NHS Tayside Medical Physics, Ninewells Hospital, Dundee, United Kingdom



http://dx.doi.org/10.1016/j.ultrasmedbio.2016.12.015

Address correspondence to: Zhihong Huang, School of Science and Engineering, Fulton Building, Dundee, DD1 4HN, UK. Tel: +441382385477. E-mail: z.y.huang@dundee.ac.uk

**Abstract- Parameters of blood flow measured by ultrasound in radial and ulnar arteries, such as flow velocity, flow rate and wall shear rate, are widely used in clinical practice and clinical research. Investigation of these measurements is useful for evaluating accuracies and providing the knowledge of error sources. A method for simulating the spectral Doppler ultrasound measurement process was developed with computational fluid dynamics providing flow-field data. Specific scanning factors were adjusted to investigate their influences on estimation of the maximum velocity waveform, and flow rate and wall shear rate were derived using the Womersley equation. The overestimation in maximum velocity increases greatly (peak systolic from about 10% to 30%, time-averaged from about 30% to 50%) when the beam-vessel angle is changed from $30^{o}$ to $70^{o}$. The Womersley equation was able to estimate flow rate in both arteries with less than 3% error, but performed better in the radial artery (2.3% overestimation) than the ulnar artery (15.4% underestimation) for estimating wall shear rate. It is concluded that measurements of flow parameters in the radial and ulnar arteries with clinical ultrasound scanners are prone to clinically significant errors.**

***Key words:*** **Computational fluid dynamics, Radial artery, Ulnar artery, Flow velocity, Flow rate, Wall shear rate, Womersley, Doppler ultrasound, Simulation, Field II.**

# INTRODUCTION

Measuring blood flow velocity (FV) and related quantities, such as flow rate (FR) and wall shear rate (WSR) with ultrasound, has been of interest for several decades in clinical practice and in clinical research (Gill 1985; Hoskins 2011). A large number of studies have concentrated on measuring and validating these parameters in various arterial sites with ultrasound (Leguy et al. 2009; Ponzini et al. 2010; Osmanski et al. 2012). Reviews of the topic are provided in Hoskins (1999b) and Hoskins (2008).

Most previous studies focused on the large arteries such as carotid or femoral where diameters are typically in the range 4-8 mm. There has been less effort in smaller arteries. Of particular interest in this paper are the radial and ulnar arteries in the wrist where the arterial diameters are typically about 2-3.5 mm. Clinical studies have used ultrasound to measure velocity related quantities in these two arteries in relation to the creation of arteriovenous fistula, in preparation for radial artery harvesting for coronary bypass surgery, and in the study of Raynaud's syndrome. For instance, the WSR or its derivative wall shear stress (WSS) has been in the remodelling of radial artery after arteriovenous fistula for haemodialysis access in many studies (e.g. Remuzzi et al. 2003; Manini et al. 2014). Furthermore, in radial artery harvesting for coronary bypass surgery, preoperative assessment of adequacy of the collateral ulnar circulation to the hand by detecting the FV or FR in the ulnar artery is necessary to avoid postoperative ischemia which could lead to severe risk (Royse et al. 2008; Habib et al. 2012). The FV and its related parameter FR also have chosen to help distinguish different types of Raynaud's syndrome. This differentiation is important for clinical management (Chikui et al. 1999; Toprak et al. 2011).

Routine clinical ultrasound scanners only provide quantitative FV (frequency shifts) with spectral Doppler from a single small sample volume. Other flow related parameters, such as FR and WSR, have to be derived based on the data from this single sample volume. Some studies simply estimated the FR as the product of maximum FV and blood vessel area (Toprak et al. 2011), and can only make a rough estimate. The Hagen-Poiseuille model was also used to estimate the FR in

early studies but this assumes the flow is steady. The Womersley theory was proposed as a more advanced method to derive the velocity profile under pulsatile flow, from which both the FR and the WSR can be calculated. Measurements of FR and WSR based on the Womersely theory using clinical ultrasound, including the evaluations of these measurements, have been conducted in large arteries such as the carotid and brachial arteries (Blake et al. 2008; Ponzini et al. 2010) and although the Womersley theory was also applied to estimate the FR and WSR in the small-diameter radial and ulnar arteries (Remuzzi et al. 2003; Van Canneyt et al. 2013), there are very few studies evaluating those measurements. Considering the value of the FR and WSR in clinical practice and research, it is felt necessary to assess this Womersley theory in these two arteries. The authors have previously reported a flow-phantom study on measurement of FR and WSR in straight vessels with diameter comparable to the radial and ulnar arteries(Zhou et al. 2016). The flow phantom in that study was not able to generate a physiologically realistic flow due to its straight tube-like blood vessel mimic.

While the traditional approach to evaluating velocity measurement errors is by use of experimental flow phantoms, a less common, but potentially more flexible method, is simulation of the ultrasound measurement process in the computer. This involves simulation of the ultrasound system and also simulation of the flow-field. Simulation of the ultrasound system involves simulation of beam-forming including scattering from seed particles, followed by construction and processing of RF data (Kerr and Hunt 1992; Jensen and Munk 1997). At this earlier date, the flow field was obtained by approximated analytical equations to derive the trajectory of moving scatterers for simulating ultrasound signals.

Computational fluid dynamics (CFD) provides 3D, time-varying, flow-field data using an iterative approach. This has been developed for simulation of patient-specific blood flow since the late 1990s (Milner et al. 1998; Taylor and Figueroa 2009; Malkawi et al. 2010) and there is a growing community using these techniques (Steinman and Taylor 2005; Hoskins and Hardman 2009; Sui et al. 2015). Swillens et al coupled ultrasound simulation with CFD in the investigation of

velocity measurement errors in arteries (Swillens et al. 2009a; Swillens et al. 2009b; Swillens et al. 2010). The meshed geometry from CFD was transformed into a 3D grid where moving scatterers were fitted spatially and temporally according to the CFD velocity field. This group reported FV and FR measurement errors in the radial artery (Van Canneyt et al. 2013), but not of WSR, and not in the ulnar artery. Furthermore, factors affecting the Doppler ultrasound estimations in these two arteries remained to be investigated.

In the present study, the technique of coupling CFD and ultrasound simulation is adopted to evaluate the errors in FV, FR and WSR measured by Doppler ultrasound in the radial and ulnar arteries.

## METHODS

### *Overall*

The basic simulation procedure to investigate the ultrasound-measured flow parameters in the radial and ulnar arteries is explained below and a schematic for this procedure is shown in Figure 1 to help conceptualise this simulation method.

- The MRI dataset from a volunteer's arm was obtained to reconstruct the 3D geometry of the radial and ulnar arteries, and provide the necessary boundary conditions for CFD simulation.
- CFD simulation was used to calculate the blood velocity field within the 3D geometry.
- Based on the CFD-calculated velocity field, simulated moving scatterers within the 3D geometry were scanned virtually by an ultrasound simulator to obtain realistic RF data.
- The RF data was used to estimate the FV by applying typical signal processing strategies that are commonly used in clinical ultrasound imaging. FR and WSR were derived based on the Womersley theory.

- Flow related parameters estimated from ultrasound were compared with the CFD reference values, giving an objective assessment of ultrasound estimations and the performance of Womersley equation in estimating FR and WSR.

*Imaged-based CFD simulation*

*MRI scanning of vascular anatomy* for *establishing 3D geometry and boundary conditions:* MRI imaging data from the left arm of a single healthy male volunteer (aged 27 years) was acquired on a 3T Magnetom Trio (Siemens, Erlangen, Germany). A 4-channel flex surface coil was wrapped around the lower arm for MR signal reception, and the volunteer was positioned head first and supine in the scanner with echocardiogram (ECG) leads on the chest. Scanning was performed on the left arm of the volunteer, and the arm was by the side of the body in a comfortable position as close as possible to the central axis of the scanner bore. Localiser images were initially acquired for anatomical orientation, followed by a high spatial resolution 3D gradient echo Multi-Echo Data Image Combination (MEDIC) sequence with water excitation acquired in the axial oblique plane (perpendicular to the long-axis of the lower arm). The images were acquired with a repetition time (TR) of 29ms, echo time (TE) of 16 ms and flip angle (FA) of $8^{o}$. A series of 176 contiguous slices, each 1.06 mm thick were acquired with an in-plane pixel resolution of 192x256 and a field of view of 135mm. The total time of the sequence was 8 minutes. A 2D time of flight (2D-TOF) MR angiography (MRA) sequence was applied in the same orientation, with TR/TE 13.0/5.80 ms and FA $18^{o}$. A series of 128 slices, each 1.50 mm thick were acquired with an in-plane pixel resolution of 192x256 and a field of view of 140mm. The total duration of this sequence was 6.5 minutes. Finally, a 2D phase contrast MRI (PCMRI) sequence was applied in the axial oblique plane in order to establish arterial and venous flow velocities for the radial and ulnar arteries. This single slice sequence (3mm thick) was acquired with TR/TE 55.80/4.91 ms and FA $30^{o}$, with 64 temporal phases acquired across the cardiac cycle. The in-plane pixel resolution was 168x192 and the field of view 127 mm. The sequence was run twice with velocity encoding (VENC) values of 65

$mm.sec^{-1}$ and $75mm.sec^{-1}$ – just above the anticipated peak arterial blood flow velocities. This study followed the local Ethical protocol and written informed consent was given by the volunteer.

*Segmentation and meshing*. Image processing of the MRI dataset was performed using Amira software (Amira 5.4.3, FEI, Hillsboro, Oregon, USA). This involved segmentation of the vessels by manually extracting the lumen-vessel boundaries in each slice of the MRI images. Surface smoothing was applied in Amira before exporting the stl (stereolithography) surface file, in an attempt to get a surface free of rough edges but with the minimum loss of the original surface detail. The region of interest from 40 mm above the bifurcation in brachial artery down to a point near the wrist was chosen. In order to achieve a fully-developed flow, both the inlet and outlet sections were extended (Fig. 2). Meshing of the 3D geometry with hexahedral elements was performed using the open source toolkit pyFormex (http://pyformex.org) by the meshing method proposed by De Santis et al. (2011). During the meshing, isoparametric transformation is used to map a parametrically defined quadrilateral surface mesh into the vessel volume after representing the lumen surface with longitudinal Bezier splines. 351288 hexahedral elements were obtained for the whole geometry after mesh independence test based on the maximum peak velocity and the maximum wall shear rate.

*CFD simulation*. Boundary conditions required for simulating the velocity field included one inlet in brachial artery, and two outlets in radial and ulnar arteries respectively, plus the vessel walls. The flow rate waveforms in brachial artery inlet and ulnar artery outlet were obtained from phase-contrast MRI images as explained and were used as corresponding inlet and outlet flow conditions for CFD. A parabolic velocity profile was assumed when using flow rate waveforms as inlet and outlet conditions. The blood pressure waveform measured by applanation tonometry (SphygmoCor XCEL PWA, AtCor Medical Pty Ltd, Illinois, USA) in the radial artery was scaled to 80-120mmHg and used for the outlet pressure boundary condition. In addition, all waveforms were scaled to one second with respect to time for conformance although the real cardiac cycles obtained at different sites from flow and pressure are not exactly one second (60 heartbeats per minute). The

specific amplitude of these waveforms are shown in Figure 2, where the time-averaged flow rate is 47.2 $ml.min^{-1}$ in the brachial inlet and 21.4 $ml.min^{-1}$ in the ulnar artery outlet within one cardiac cycle (obtained from phase-contrast MRI as explained). The 3D geometry was assumed to have rigid walls and the no-slip condition was applied to at the walls. One and a half cardiac cycles were simulated to more than cover a complete cardiac cycle.

Blood was assumed to be a non-compressible, Newtonian fluid having the typical properties of normal healthy human's blood, density 1050 $kg.m^{-3}$ and dynamic viscosity 3.5 mPa.s (Stewart et al. 2012). Abaqus/CFD (Simula, Inc. Providence, RI, USA) was chosen to solve the Navier-Stokes equations in the 3D transient domain. The projection method in Abaqus/CFD was used to enable segregation of pressure and velocity fields for efficient solution, and a second-order least-squares gradient estimation was used for numerical solution. The time step for results output was set to 5 ms. This meant 200 values were available for the velocity variable within one cardiac cycle. To save simulation time, only the sections near insonating positions (as indicated by R and U in Fig. 2) were chosen to generate velocity field output. The CFD simulation took 11 hours on a PC with 64-bit, 3.40 GHz Intel Core i7-3770 processor.

*Ultrasound imaging simulation*

The Field II ultrasound simulator was used to simulate the PW Doppler ultrasound. 'Field II operates by simulation of an acoustic field, both in transmission and reception. The received RF data is then available for estimation of flow velocity (Jensen and Svendsen 1992; Jensen 1996). In Field II generic beam forming was accomplished by calculating the time delays of transmitting and receiving signals for individual elements according to the area of interest. There was no attempt to replicate the beam-forming of any particular commercial ultrasound system; instead generic beam forming was undertaken. The acoustic field generated by the Field II has high reported accuracy when compared with realistic measured acoustic field (Jensen 1990).

A linear-array transducer was created in Field II for transmitting and receiving the ultrasound waves. Parameters of this transducer are listed in Table 1. Each transducer element was divided into 4 rectangular elements in elevation. The pulse repetition frequency (PRF) varied from 3 kHz to 10 kHz according to the velocity in the vessels under different circumstances. Since an accurate acoustic field cannot be guaranteed in the near-field region of the simulated sound field in Field II(Jensen and Svendsen 1992), imaging depths were set between 4-50 mm to investigate its effect and to make sure the sample volume was located in the far-field area while looking into other factors. The transmit focus was set to the center of the sample volume which is located at the central axis of the virtual blood vessel. The scanning positions for the radial and ulnar arteries are indicated as R and U in Figure 2. The length of the sample volume was set large enough (2.3 mm) to encompass maximum velocity.

*Inputting CFD velocity field to US simulator*

Field II simulates the RF signal based on the moving point scatterers within the sample volume. The trajectories of these were determined by the flow velocity field from CFD. The method proposed by Swillens et al. (2009b) was applied here to regulate stepwise movement of the scatterers which are spatially and temporally fitted into the meshed 3D grid. The concentration depended on the spatial cell resolution of the sound beam, normally 10 scatterers in cubic resolution cell (Thijssen 2003; Swillens et al. 2009b).

*Procedure and protocol*

To investigate FV and related FR and WSR in these two arteries, the following steps were taken:

- Based on the simulated RF data, conventional IQ demodulation and fast Fourier transformation were used to estimate the velocity spectral sonogram;
- The maximum blood velocity waveform was obtained from the outline of the sonogram;

- The Womersley equation was used to estimate the velocity profile in the blood vessels based on the maximum velocity waveform from the PW sonogram and vessel diameter from 3D geometry (Womersley 1955; Zhou et al. 2016);
- FR and WSR then can be derived from the velocity profile and arterial diameter;
- The FV, FR and WSR estimated from simulated RF data can finally be compared with their corresponding values from CFD results; the WSR results were available from the velocity value closest to the vessel wall and its distance from the wall surface in the CFD velocity field.

The accuracy of estimated FV was investigated under beam-vessel angles of 30 °, 40°, 50 °, 60 °, and 70 ° by placing the synthetic blood vessel at the appropriate angle with respect to the sound beam propagation direction. The flow rate in the blood vessel was set at different levels to investigate its effect on the ultrasound maximum velocity estimation, ranging from two thirds to twice the phased-contrast MRI measurement by changing the amplitude of the boundary conditions (flow rate waveforms in Fig. 2) during CFD simulation. To avoid the influence caused by near-field approximation in field II, the imaging depth was varied as follows: 4 mm, 10 mm, 20 mm, 30 mm, 40 mm and 50 mm. The effect of the beam-vessel angle, the flow rate and the imaging depth were each investigated by adopting a standard set of criteria then varying each in turn. The standard criteria is 60 ° for beam-vessel angle, MRI-measured value for flow rate and 40 mm for imaging depth. For example, flow rate and imaging depth would be fixed at MRI-measured value and 40 mm respectively when investigating beam-vessel angles from 30 ° to 70 °.

Using the Field II ultrasound scanning was repeated five times in each case when measuring the maximum velocity so that the mean values and standard deviations were obtained for these estimations. Maximum velocity waveform from five individual measurements were averaged to calculate FR and WSR, with beam-vessel angle of 60°, MRI-measured flow rate and imaging depth of 40 mm.

## RESULTS

*Flow Velocity*

The velocity field at the peak systolic point of the cardiac cycle in the transverse plane where the beam axis passes through is shown in Figure 3. It can be seen that the velocity in the radial artery is higher than in the ulnar artery, with a peak systolic velocity of over 0.6 $m.s^{-1}$. The velocity profiles also differ. Sample volume positions in the PW Doppler ultrasound image are marked in the transverse plane (Fig. 3).

The diameters of radial and ulnar arteries at the beam axis were measured as 3.22±0.02 mm and 2.82±0.02 mm respectively from the 3D geometry. Simulated velocity spectral sonogram, based on the velocity field calculated from CFD, are shown in Figure 4. Maximum velocity waveforms, extracted from the spectrum, are superposed onto the PW sonogram.

Ultrasound-measured maximum velocity waveforms were compared with CFD maximum velocity waveforms in two methods. Maximum velocity waveforms in the radial artery from CFD and ultrasound in the beam direction are compared in Figure 5a, with the beam-vessel angle at $60^{o}$. The CFD maximum velocity waveforms in the direction parallel to the vessel are compared with ultrasound-measured waveforms in the direction of vessel axis as well according to the 60-degree beam-vessel angle (Fig. 5b). Similar comparisons for the ulnar artery are shown in Figure 5c and Figure 5d. In the radial artery the ultrasound overestimation of maximum velocity waveform in the beam direction (30.9% for systolic peak velocity and 52.6% for time-averaged velocity) is higher than that in the angle-corrected vessel direction (24.2% for systolic peak velocity and 43.6% for time-averaged velocity). This overestimation difference between beam direction and vessel direction is much smaller in the ulnar artery where they are 20.6% and 20.9% (Fig. 5c and 5d) for systolic peak velocity, and 39.6% and 40.4% for time-averaged velocity.

Based on the maximum velocity waveforms in CFD, errors in the systolic peak velocity and time-averaged velocity of the ultrasound estimated maximum velocity waveform are illustrated at different beam-vessel angles, flow rate and imaging depths (Fig. 6a to Fig. 6f). While changing the flow rate in CFD from two thirds to two times of the MRI-measured values, the error percentages in both arteries (Fig. 6a and 6b) are almost constant. However the beam-vessel angle does have an obvious effect on the maximum velocity estimation (Fig. 6c and 6d). In Figure 6e and 6f, it is seen the imaging depth has no effect for the radial artery but a very large effect in estimation of the maximum velocity waveform.

*Flow rate*

Figure 7a presents FR waveforms derived from virtually ultrasound-measured maximum velocity waveforms using the Womersley equation. The estimated time-averaged flow rate from ultrasound is 37.9 $ml.min^{-1}$ in the radial artery and 29.2 $ml.min^{-1}$ in the ulnar artery. With reference to the time-averaged flow rates of 25.8 $ml.min^{-1}$ in the radial artery and 21.4 $ml.min^{-1}$ in the ulnar artery for boundary conditions in CFD, the ultrasound-estimated time-averaged flow rates were overestimated by 46.9% and 36.3% in the radial and ulnar arteries respectively. FR waveforms derived from CFD maximum velocity waveforms using Womersley equation are given in Figure 8a. In this case, the time-averaged flow rates from Womesley equations are 26.3 $ml.min^{-1}$ for the radial artery and 20.8 $ml.min^{-1}$ for ulnar artery, indicating very small errors compared to the true value from CFD.

*Wall shear rate*

The WSR was also analysed in two ways. The WSR waveforms calculated from the virtually ultrasound-measured maximum velocity waveforms and from the CFD maximum velocity waveforms were both compared with that from the CFD references in the two arteries (Fig. 7b and Fig. 7c, Fig. 8b and 8c). The CFD reference WSR waveforms at each meshed element (elements are

shown in Fig. 9 for the radial artery) around a circumference of the vessel wall at the axis of the sound beam were calculated. It can be seen that the wall shear rate values are not constant around the circumference. The average WSR waveform was calculated around this circumference in each case to compare with Womersley-estimated WSR waveform in terms of their systolic peak values and time-averaged values as shown in Table 2.

## DISCUSSION

Blood flow in arteries is complicated due to the characteristics of the cardiovascular system such as its geometry and pulsatile flow. In modern clinical ultrasound scanners, a dominant source of error velocity estimation is the geometric spectral broadening which can lead to overestimation in velocity especially for maximum, and its error is dependent on the beam-flow angle (Hoskins 1996; Steinman et al. 2001). In PW Doppler a lack of knowledge of the true beam-flow angle (the angle between the beam and moving target) can cause underestimation or overestimation of flow velocity in the direction of vessel axis when simply assuming the flow is parallel to blood vessel(Hoskins 1999a; Van Canneyt et al. 2013). The bias in estimating FV would cause errors in estimating the velocity related parameters, such as FR and WSR.

### *Flow velocity*

In Figure 3, the velocity contours in the transverse planes of these two arteries, where sample volumes are located, showed that the flow conditions in the radial artery are more complicated and the velocity profile is not symmetric compared to that in the ulnar artery. This also showed that even a long sample volume could not guarantee the maximum velocity is located within when the velocity profile is not symmetric.

Due to the asymmetric velocity profile, the overestimations in maximum velocity waveforms in the radial artery were quite different in the beam direction (30.9% for systolic and 52.6% for time-averaged) and in the blood vessel direction (24.2% for systolic and 40.4% for time-averaged) as shown in Figure 5a and 5b. Note that the velocity in the vessel direction from ultrasound was estimated based on the velocity in beam direction and the beam-vessel angle. The difference is caused by the inconsistency between the direction of blood flow and the direction parallel to the blood vessel. This is more prevalent under a complicated flow condition (Hoskins 1999a; Van Canneyt et al. 2013). As the flow in the ulnar artery is more symmetric (Fig. 3), this less complicated flow condition keeps the overestimation difference very small between the beam direction (20.6% for systolic and 39.6% for time-averaged) and vessel axis direction (20.9% for systolic and 40.4% for time-averaged).

Compared to the error generated by the angle variation, the error caused by different beam-vessel angles was more severe. When changing the beam-vessel angle from $30^{o}$ to $70^{o}$ degrees, overestimation of both the systolic peak velocity and the time-averaged velocity in the maximum velocity waveforms increased drastically from about 10% to 50% in both arteries (Fig. 6c and 6d). Overestimation percentage errors in the time-averaged velocity were higher than that in the systolic peak velocity. This angle-dependent overestimation in maximum velocity by simulation in this study is in agreement with previous phantom and in *vivo* studies, and was believed to be caused by the geometric spectral broadening (Hoskins 1996; Tola and Yurdakul 2006; Hoskins et al. 2010). It is noted that the angle that really matters in velocity overestimation caused by geometric spectral broadening is the angle between sound beam and the true flow direction(Hoskins 1999a). In this study, this true beam-flow angle changes as a result of changing the beam-vessel angle.

From Figure 6a and 6b, it was found that the amplitude of flow rate in the vessel does not influence the ultrasound estimation of velocity. When the flow rate in the CFD was set from two thirds to twice the MRI measured value, the overestimation of FV stays almost constant and is governed by the $60^{o}$ beam-vessel angle. In the Field II simulator, the accuracy of the simulated

acoustic field can only be guaranteed in the far-field region. The far-field region which is about 1.3 mm in this study based on $l >> w^2/(4\lambda)$, where $l$ is the distance to the field point, $w$ the largest dimension of the rectangle in element and $\lambda$ the wavelength (Jensen and Svendsen 1992). When the imaging depth in the ulnar artery was adjusted from 4 mm to 50 mm, the estimated systolic peak velocity and time-averaged velocity changed markedly initially, and then stayed constant after 40 mm (Fig. 6f). Although the imaging depth does not affect the velocity estimation in the radial artery (Fig. 6e), it was still set to a constant 40 mm in all the simulations in this study.

It should be noted that the velocity field acting as a basis for the moving scatterers in the synthetic blood vessel was simulated by the CFD which uses the blood flow rates and arterial 3D geometry as boundary conditions. The resolution and accuracy of measurements from MRI could affect the results of the simulated velocity field in CFD. The CFD velocity field then might not be exactly the same as the real velocity field in the scanned volunteer. Despite this, the velocity field in CFD is far more realistic than the flow conditions generated in conventional experimental flow phantoms and this image-based CFD simulation currently remains the main means to obtain the patient-specific hemodynamic parameters (Taylor and Figueroa 2009; Taylor and Steinman 2010).

*Flow rate*

Compared to the time-averaged FR used in the boundary conditions for CFD simulation, there are obvious overestimation in the ultrasound-measured results. The 46.9% and 36.3% overestimation in time-averaged flow rates in the radial and ulnar arteries, calculated from the FR waveforms shown in Figure 7a, were caused by the overestimation in ultrasound-measured maximum velocity waveforms.

The time-averaged FR could be accurately estimated based on the CFD maximum velocity instead of the ultrasound-measured maximum velocity. In this case the time-averaged flow rates, calculated from the FR waveforms shown in Figure 8a, are 26.3 $ml.min^{-1}$ in the radial artery and 20.8 $ml.min^{-1}$ in the ulnar artery, with very small differences compared to the CFD reference where

time-averaged flow rates are 25.8 ml.min$^{-1}$ and 21.4 ml.min$^{-1}$ in these two arteries respectively. Therefore, the Womersley theory is able to estimate the time-averaged FR in both arteries on the condition that the maximum velocity waveforms are provided accurately.

*Wall shear rate*

The Womersley equation assumes that the blood vessel is an ideal tube and the flow profile is symmetric, meaning WSR values would be the same around a circumference on the vessel wall. This assumption is not true in reality. The WSR calculated from near-wall velocity gradient in CFD (reference value) in this study showed that WSR values vary with position around the vessel wall, especially during the systolic period of the cardiac cycle. Results in Table 2 show that the Womersley equation is able to estimate WSR waveform (averaged waveform around a circumference) in the radial artery in terms of the systolic peak and time-averaged WSR if the correct velocity waveform is used. The overestimations (peak: 1273 s$^{-1}$ vs 1078.3 s$^{-1}$, time-averaged: 191.2 s$^{-1}$ vs 135.6 s$^{-1}$) occur only when the ultrasound-overestimated maximum velocity waveforms were used, and there is only minor overestimation if maximum velocity waveform from the CFD itself. That is not the case in the ulnar artery where the WSR waveform was not overestimated as in the radial artery even though the overestimated maximum velocity waveform from ultrasound was used. The Womersley equation seems partly to compensate for the overestimation in velocity. When the maximum velocity waveform from CFD velocity field was used, both systolic peak and time-averaged WSR were then underestimated by the Womersley equation.

It was shown that the performance of the Womersley equation in estimating WSR is dependent on the flow condition in the arteries and cannot guarantee the Womersley equation would perform better under a more symmetric flow. Actually it could be worse as it is in the ulnar artery in this study.

## CONCLUSION

With the flexible simulation platform, the FV, FR and WSR were investigated under realistic flow conditions in the radial and ulnar arteries. The errors in estimating maximum velocity waveforms using Doppler ultrasound due to different sources of error were confirmed by simulation for the first time. Furthermore, the performance of the Womersley equation was proved to vary under different flow conditions in these two arteries. Since errors in those measurements can lead to misinterpretation, this study should raise the awareness of researchers and clinicians who need to use these measurements in these two arteries, such as in preoperative assessment of adequacy of the collateral ulnar circulation for coronary bypass surgery, in evaluation of the radial artery remodelling after creation of arteriovenous fistula for haemodialysis access, and to distinguish the types of Raynaud's syndrome for clinical management.

## ACKNOWLEDGEMENTS

This work is supported by China Scholarship Council (CSC) and University of Dundee. The authors gratefully acknowledge Dr Efstratios Kokkalis for his suggestions on Computational Fluid Dynamics at the beginning of this simulation method development and his assistance of obtaining valid MRI images.

REFERENCES

Blake JR, Meagher S, Fraser KH, Easson WJ, Hoskins PR. A method to estimate wall shear rate with a clinical ultrasound scanner. Ultrasound in Medicine & Biology 2008;34:760-74.

Chikui T, Izumi M, Eguchi K, Kawabe Y, Nakamura T. Doppler spectral waveform analysis of arteries of the hand in patients with Raynaud's phenomenon as compared with healthy subjects. Am J Roentgenol 1999;172:1605-9.

De Santis G, De Beule M, Segers P, Verdonck P, Verhegghe B. Patient-specific computational haemodynamics: generation of structured and conformal hexahedral meshes from triangulated surfaces of vascular bifurcations. Comput Methods Biomech Biomed Engin 2011;14:797-802.

Gill RW. Measurement of blood flow by ultrasound: accuracy and sources of error. Ultrasound Med Biol 1985;11:625-41.

Habib J, Baetz L, Satiani B. Assessment of collateral circulation to the hand prior to radial artery harvest. Vasc Med 2012;17:352-61.

Hoskins PR. Accuracy of maximum velocity estimates made using Doppler ultrasound systems. Brit J Radiol 1996;69:172-7.

Hoskins PR. A comparison of single- and dual-beam methods for maximum velocity estimation. Ultrasound Med Biol 1999a;25:583-92.

Hoskins PR. A Review of the Measurement of Blood Velocity and Related Quantities Using Doppler Ultrasound. 1999b;

Hoskins PR. Simulation and Validation of Arterial Ultrasound Imaging and Blood Flow. Ultrasound in Medicine & Biology 2008;34:693-717.

Hoskins PR. Estimation of blood velocity, volumetric flow and wall shear rate using Doppler ultrasound. Ultrasound 2011;19:120-9.

Hoskins PR, Hardman D. Three-dimensional imaging and computational modelling for estimation of wall stresses in arteries. Brit J Radiol 2009;82:S3-S17.

Hoskins PR, Soldan M, Fortune S, Inglis S, Anderson T, Plevris J. Validation of Endoscopic Ultrasound Measured Flow Rate in the Azygos Vein Using a Flow Phantom. Ultrasound Med Biol 2010;36:1957-64.

Jensen JA. Field: A program for simulating ultrasound systems. Med Biol Eng Comput 1996;34:351-3.

Jensen JA, Munk P. Computer phantoms for simulating ultrasound B-mode and CFM images. Acoust Imag 1997;23:75-80.

Jensen JA, Svendsen NB. Calculation of pressure fields from arbitrarily shaped, apodized, and excited ultrasound transducers. IEEE Trans Ultrason Ferroelectr Freq Control 1992;39:262-7.

Kerr AT, Hunt JW. A method for computer simulation of ultrasound Doppler color flow images--II. Simulation results. Ultrasound Med Biol 1992;18:873-9.

Leguy CA, Bosboom EM, Hoeks AP, van de Vosse FN. Assessment of blood volume flow in slightly curved arteries from a single velocity profile. J Biomech 2009;42:1664-72.

Malkawi AH, Hinchliffe RJ, Xu Y, Holt PJ, Loftus IM, Thompson MM. Patient-specific biomechanical profiling in abdominal aortic aneurysm development and rupture. J Vasc Surg 2010;52:480-8.

Manini S, Passera K, Huberts W, Botti L, Antiga L, Remuzzi A. Computational model for simulation of vascular adaptation following vascular access surgery in haemodialysis patients. Comput Methods Biomech Biomed Engin 2014;17:1358-67.

Milner JS, Moore JA, Rutt BK, Steinman DA. Hemodynamics of human carotid artery bifurcations: computational studies with models reconstructed from magnetic resonance imaging of normal subjects. J Vasc Surg 1998;28:143-56.

Osmanski BF, Pernot M, Montaldo G, Bel A, Messas E, Tanter M. Ultrafast Doppler Imaging of Blood Flow Dynamics in the Myocardium. IEEE Trans Med Imaging 2012;31:1661-8.

Ponzini R, Vergara C, Rizzo G, Veneziani A, Roghi A, Vanzulli A, Parodi O, Redaelli A. Womersley number-based estimates of blood flow rate in Doppler analysis: in vivo validation by means of phase-contrast MRI. IEEE transactions on bio-medical engineering 2010;57:1807-15.

Remuzzi A, Ene-Iordache B, Remuzzi G. Radial artery wall shear stress evaluation in patients with arteriovenous fistula for hemodialysis access. 2003;

Royse AG, Chang GS, Nicholas DM, Royse CF. No late ulnar artery atheroma after radial artery harvest for coronary artery bypass surgery. Ann Thorac Surg 2008;85:891-5.

Steinman AH, Tavakkoli J, Myers JG, Cobbold RSC, Johnston KW. Sources of error in maximum velocity estimation using linear phased-array Doppler systems with steady flow. Ultrasound Med Biol 2001;27:655-64.

Steinman DA, Taylor CA. Flow imaging and computing: Large artery hemodynamics. Annals of biomedical engineering 2005;33:1704-9.

Stewart SFC, Paterson EG, Burgreen GW, Hariharan P, Giarra M, Reddy V, Day SW, Manning KB, Deutsch S, Berman MR, Myers MR, Malinauskas RA. Assessment of CFD Performance in Simulations of an Idealized Medical Device: Results of FDA's First Computational Interlaboratory Study. Cardiovascular Engineering and Technology 2012;3:139-60.

Sui B, Gao P, Lin Y, Jing L, Sun S, Qin H. Hemodynamic parameters distribution of upstream, stenosis center, and downstream sides of plaques in carotid artery with different stenosis: a MRI and CFD study. Acta Radiol 2015;56:347-54.

Swillens A, De Schryver T, Lovstakken L, Torp H, Segers P. Assessment of numerical simulation strategies for ultrasonic color blood flow imaging, based on a computer and experimental model of the carotid artery. Annals of biomedical engineering 2009a;37:2188-99.

Swillens A, Degroote J, Vierendeels J, Lovstakken L, Segers P. A simulation environment for validating ultrasonic blood flow and vessel wall imaging based on fluid-structure interaction simulations: ultrasonic assessment of arterial distension and wall shear rate. Med Phys 2010;37:4318-30.

Swillens A, Lovstakken L, Kips J, Torp H, Segers P. Ultrasound simulation of complex flow velocity fields based on computational fluid dynamics. IEEE Trans Ultrason Ferroelectr Freq Control 2009b;56:546-56.

Taylor CA, Figueroa CA. Patient-Specific Modeling of Cardiovascular Mechanics. Annual Review of Biomedical Engineering 2009;11:109-34.

Taylor CA, Steinman DA. Image-Based Modeling of Blood Flow and Vessel Wall Dynamics: Applications, Methods and Future Directions. Annals of biomedical engineering 2010;38:1188-203.

Thijssen JM. Ultrasonic speckle formation, analysis and processing applied to tissue characterization. Pattern Recogn Lett 2003;24:659-75.

Tola M, Yurdakul M. Effect of Doppler angle in diagnosis of internal carotid artery stenosis. J Ultrasound Med 2006;25:1187-92.

Toprak U, Hayretci M, Erhuner Z, Tascilar K, Ates A, Karaaslan Y, Karademir MA. Dynamic Doppler Evaluation of the Hand Arteries to Distinguish Between Primary and Secondary Raynaud Phenomenon. Am J Roentgenol 2011;197:W175-W80.

Van Canneyt K, Swillens A, Lovstakken L, Antiga L, Verdonck P, Segers P. The accuracy of ultrasound volume flow measurements in the complex flow setting of a forearm vascular access. J Vasc Access 2013;14:281-90.

Womersley JR. Method for the Calculation of Velocity, Rate of Flow and Viscous Drag in Arteries When the Pressure Gradient Is Known. J Physiol-London 1955;127:553-63.

Zhou X, Xia C, Khan F, Corner GA, Huang Z, Hoskins PR. Investigation of Ultrasound-Measured Flow Rate and Wall Shear Rate in Wrist Arteries Using Flow Phantoms. Ultrasound in Medicine & Biology 2016;42:815-23.

Figures.

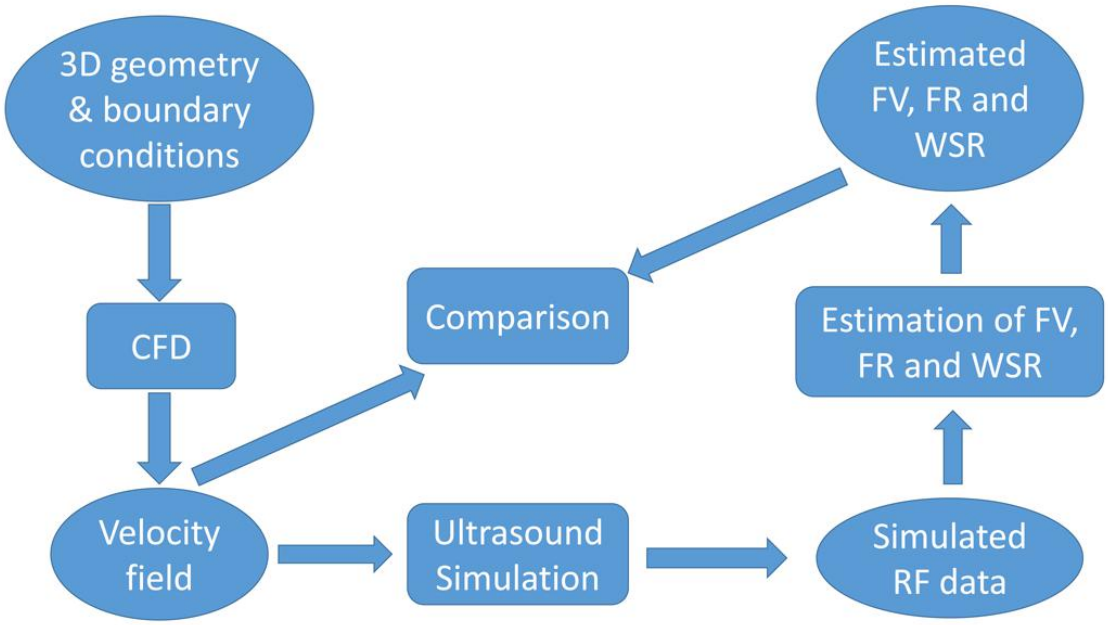


Fig. 1. Schematic diagram of the simulation method.

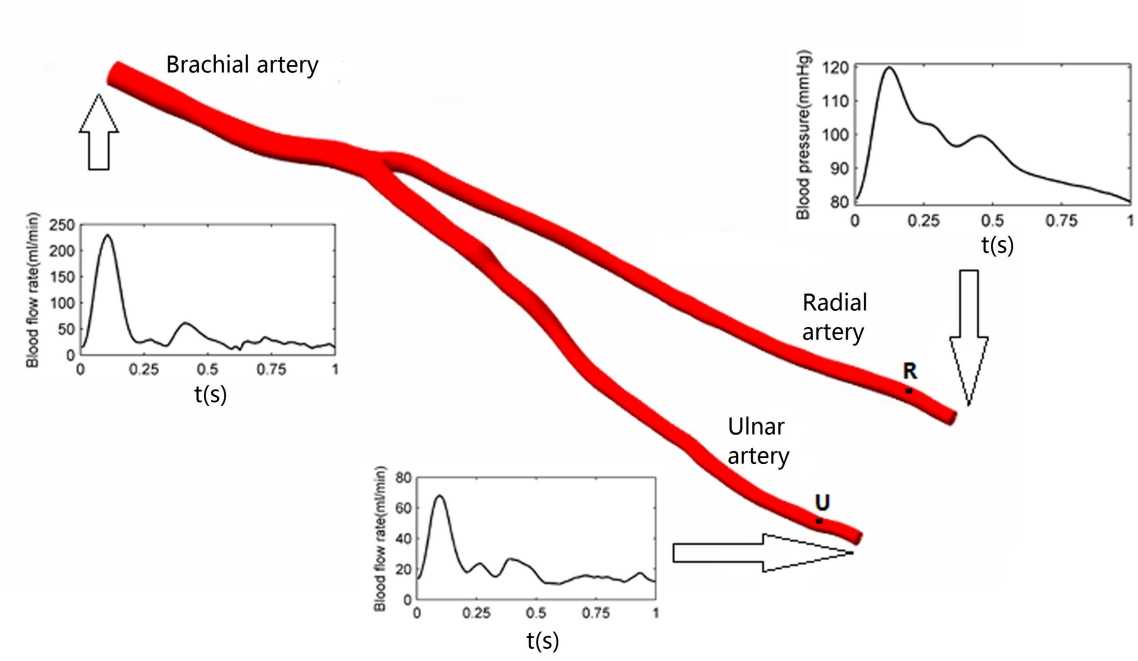


Fig. 2. 3D geometry and boundary conditions for computational fluid dynamics.

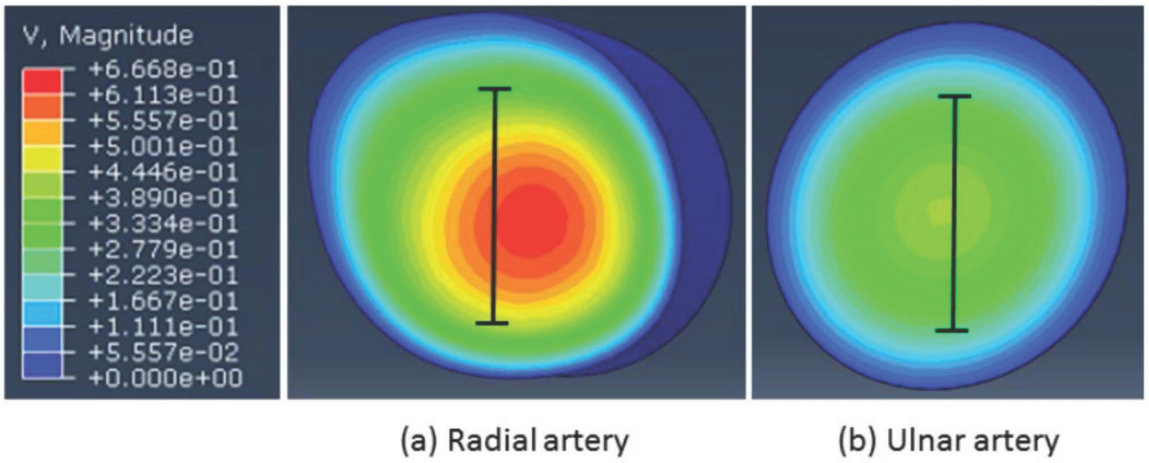


Fig. 3. Contours of flow velocity in the cross-sectional plane

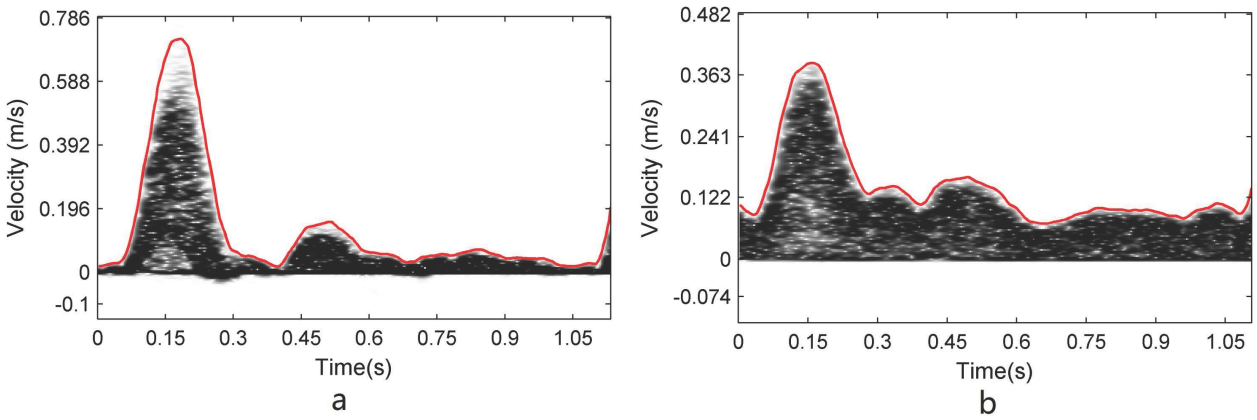


Fig. 4. PW sonograms and the maximum velocity waveforms. (a) for the radial artery. (b) for the ulnar artery.

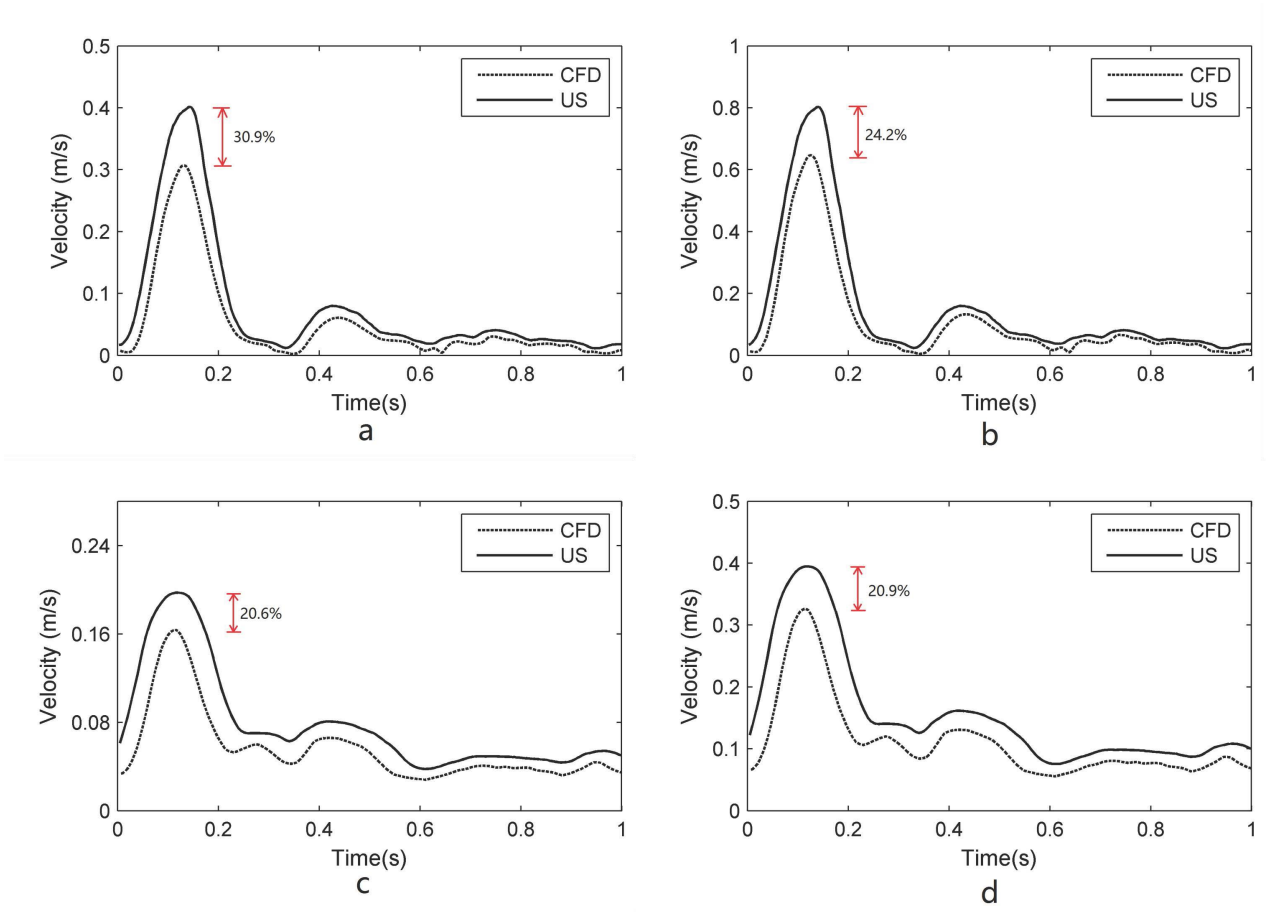


Fig. 5. Maximum velocity estimated from the ultrasound simulation and the reference result from the CFD. (a) FV waveforms in beam direction in the radial artery. (b) FV waveforms in vessel axis direction in the radial artery. (c) FV waveforms in beam direction in the ulnar artery. (d) FV waveforms in vessel axis direction in the ulnar artery. FV=flow velocity, CFD=computational fluid dynamics, US=ultrasound.

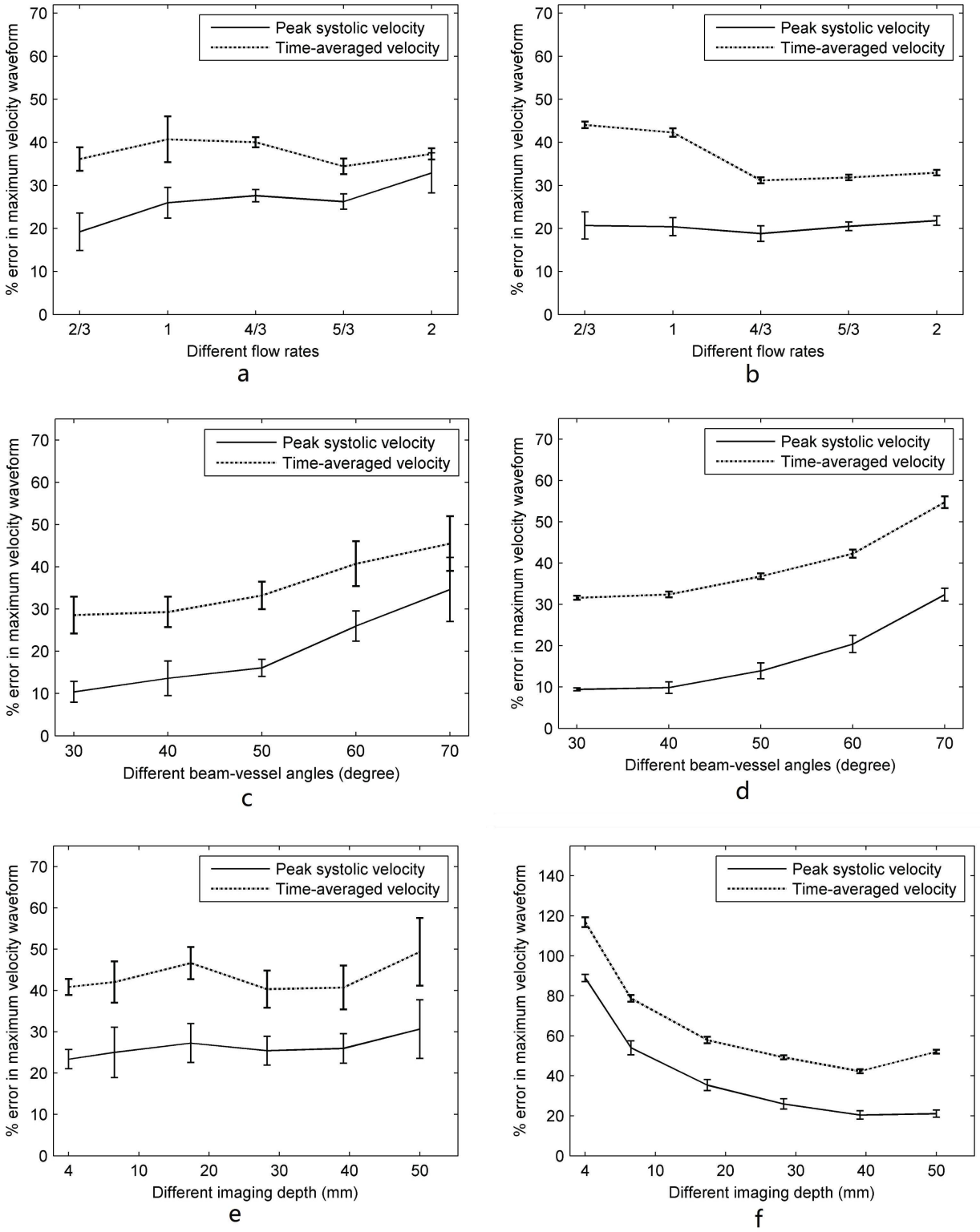


Fig. 6. Percentage errors of peak systolic and time-averaged velocity with different flow rate amplitudes, beam-vessel angles and imaging depths. (a)-(c)-(e) for the radial artery and (b)-(d)-(f) for the ulnar artery.

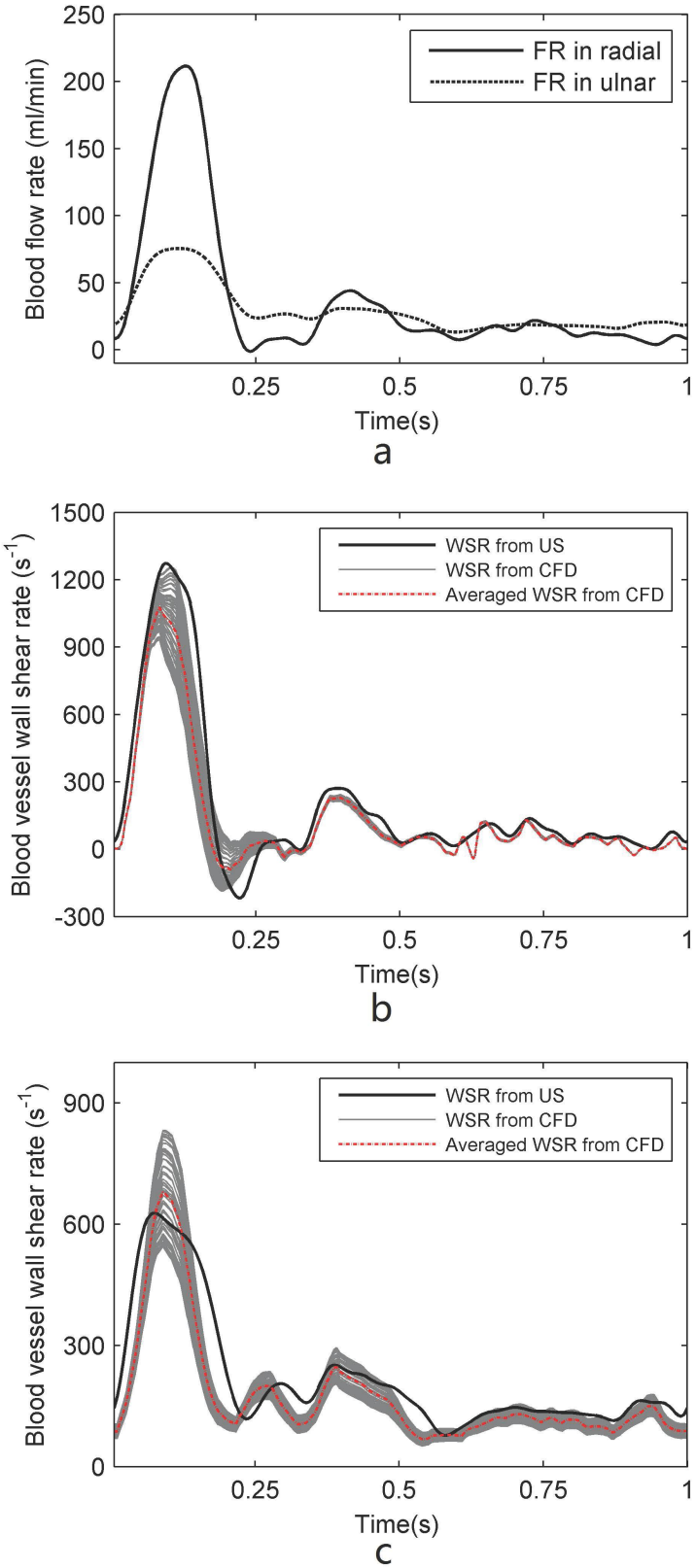


Fig. 7. FR and WSR estimated from ultrasound and from the CFD. (a) FR waveforms estimated from ultrasound-measured maximum velocity waveforms; (b)-(c) the ultrasound-measured WSR waveform; the CFD reference WSR waveforms at different sites of a circumference; and the averaged WSR waveform in CFD along this circumference; (b) for the radial artery and (c) for the ulnar artery. FR=flow rate, WSR=wall shear rate, CFD=computational fluid dynamics, US=ultrasound.

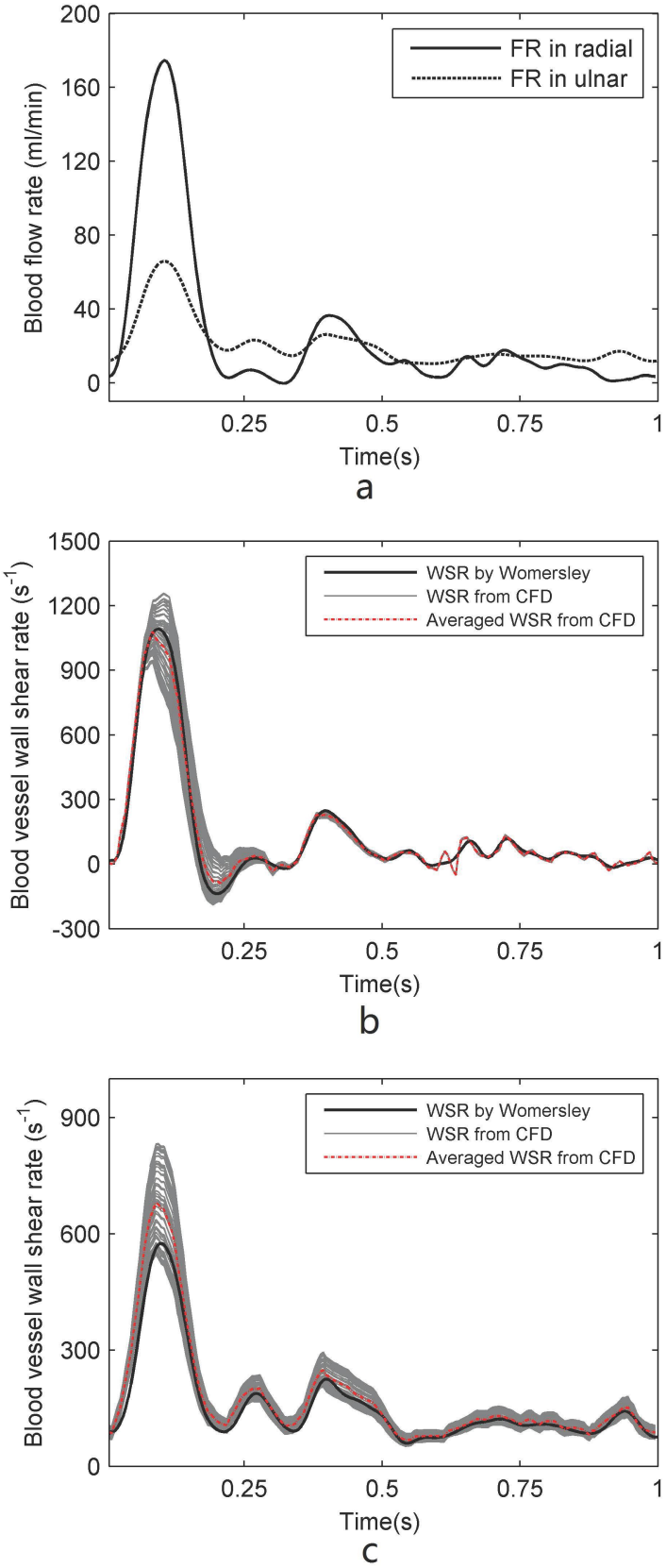


Fig. 8. FR and WSR estimated from the CFD. (a) FR waveforms estimated from CFD maximum velocity waveforms. (b)-(c) the WSR waveform estimated from CFD maximum velocity waveform; the CFD reference WSR waveforms at different site of a circumference; and the averaged WSR waveform in CFD along this circumference; (b) for the radial artery and (c) for the ulnar artery. FR=flow rate, WSR=wall shear rate, CFD=computational fluid dynamics.

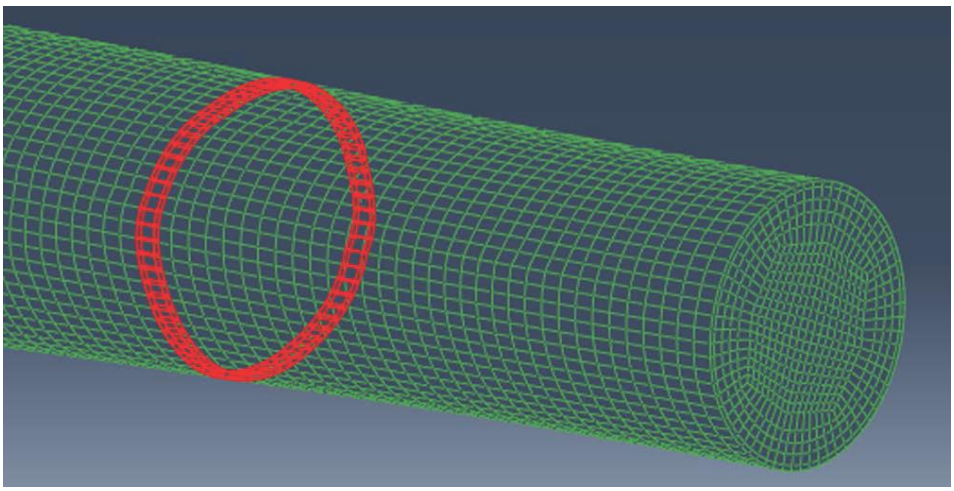

Fig. 9. Elements chosen around a circumference for calculating wall shear rate.

Tables.

Table 1. Linear array transducer settings in Field II

| Parameters | Values |
|---|---|
| Pulse central frequency ($f_0$) | 5 MHz |
| Excitation pulse (P) | Sinusoid |
| Pulse cycles (n) | 5 |
| Sound velocity (c) | 1540 m/s |
| RF data sampling frequency ($f_s$) | 100 MHz |
| Element width (w) | Half a wavelength |
| Element height (h) | 5 mm |
| Gap between elements (Kerf) | 0.05 mm |
| Number of elements (N) | 64 |
| Pulse repetition frequency (PRF) | 3-10 kHz |
| Transmit focus (F) | [0,0,4-50] mm |

Table 2. WSR ($s^{-1}$) calculated from ultrasound-based and CFD-based maximum velocity waveform

| | US-based estimations with WE | | CFD-based estimations with WE | | Reference from CFD velocity field | |
|---|---|---|---|---|---|---|
| | Systolic peak | Time-averaged | Systolic peak | Time-averaged | Systolic peak | Time-averaged |
| Radial artery | 1273.0 | 191.2 | 1103.2 | 132.4 | 1078.3 | 135.6 |
| Ulnar artery | 627.4 | 218.5 | 575.3 | 156.0 | 679.8 | 176.6 |

WSR= wall shear rate, CFD=computational fluid dynamics, WE=Womersley equation